
Policy Contrastive Decoding for Robotic Foundation Models

Shihan Wu^{1*} Ji Zhang^{2*} Xu Luo¹ Junlin Xie¹
 Jingkuan Song³ Heng Tao Shen³ Lianli Gao^{1†}

¹University of Electronic Science and Technology of China

²Southwest Jiaotong University

³Tongji University

shihan.wu.koorye@outlook.com, juana.alian@gmail.com

Abstract

Robotic foundation models, or generalist robot policies, hold immense potential to enable flexible, general-purpose and dexterous robotic systems. Despite their advancements, our empirical experiments reveal that existing robot policies are prone to learning *spurious correlations* from pre-training trajectories, adversely affecting their generalization capabilities beyond the training data. To tackle this, we propose a novel **Policy Contrastive Decoding (PCD)** approach, which redirects the robot policy’s focus toward object-relevant visual clues by contrasting action probability distributions derived from original and object-masked visual inputs. As a training-free method, our PCD can be used as a *plugin* to improve different types of robot policies without needing to finetune or access model weights. We conduct extensive experiments on top of three open-source robot policies, including the autoregressive policy OpenVLA and the diffusion-based policies Octo and π_0 . The obtained results in both simulation and real-world environments prove PCD’s flexibility and effectiveness, e.g., PCD enhances the state-of-the-art policy π_0 by **8%** in the simulation environment and by **108%** in the real-world environment. Code and demos are publicly available at: <https://Koorye.github.io/proj/PCD>.

1 Introduction

Recent efforts in developing flexible, general-purpose, and dexterous robotic systems have largely focused on robotic foundation models, or generalist robot policies. The overarching goal of such policies is to empower users to instruct robots to perform arbitrary tasks, enabling autonomous task execution with minimal human supervision. Specifically, the policy takes as input a visual observation of the robot’s state combined with a language instruction that defines the task, and outputs a robot action, such as end-effector displacement. Ongoing advancements in scaling real-world robotic data corpora have facilitated the development of numerous robot policies [4, 20, 32, 36], which have demonstrated exceptional effectiveness in controlling various robots across diverse environments and acquiring a wide range of manipulation skills.

Despite their notable achievements, existing robot policies are prone to learning *spurious correlations* [49, 13, 25] from pre-training trajectories, adversely affecting their ability to generalize outside their training data. As illustrated in Fig. 1, the robot policy predominantly relies on spurious features (e.g., background or textures) rather than object features within observations to predict actions (see **(a)(d)**). Consequently, slight alterations to the visual observation background, like adjustments to the panning light region (i.e., **(a)**→**(b)**) and the handle position (i.e., **(a)**→**(c)**), lead to **36%** and

*Equal contribution

†Corresponding author

32% drops in the policy’s action prediction performance, respectively. Prior work in other fields has demonstrated that models relying on spurious correlations often suffer significant performance degradation on test data when a distribution shift occurs between the training and test environments [31, 44, 17]. This underscores the importance of redirecting robot policies’ focus from spurious features to object-relevant ones to enhance their generalization across different scenarios during inference. Therefore, we provide a first study on the following question:

Can we propose a training-free, plug-and-play approach to mitigate the adverse effects of spurious correlations, thereby rectifying predicted actions for existing robot policies?

In this work, we present a Policy Contrastive Decoding (**PCD**) approach to answer the question. The core idea of our PCD approach is to shift the robot policy’s attention from spurious features to object-relevant ones by contrasting action probability distributions derived from original and object-masked observation images during inference. To ensure both effectiveness and flexibility of the approach, a *Tracking-to-Mask (Track2Mask)* strategy is introduced, which first annotates target-specific objects in the *initial* visual observation using human expertise (e.g., Point and Box prompts) or off-the-shelf object detection models (e.g., Grounding DINO [28]), then employs the SAM2 [21] model to track these objects across subsequent observations in the trajectory. This enables precise object masking with minimal or no human intervention. Moreover, unlike autoregressive policies, diffusion-based policies cannot directly generate action probability distributions to feed into our PCD. To cope with this limitation, we introduce a *KDE-based Probabilistic Modeling (KDE-PM)* scheme, which calculates action probability distributions for diffusion-based policies using the kernel density estimation (KDE) [47] technique. This enables our PCD approach to be compatible with both autoregressive and diffusion-based policies.

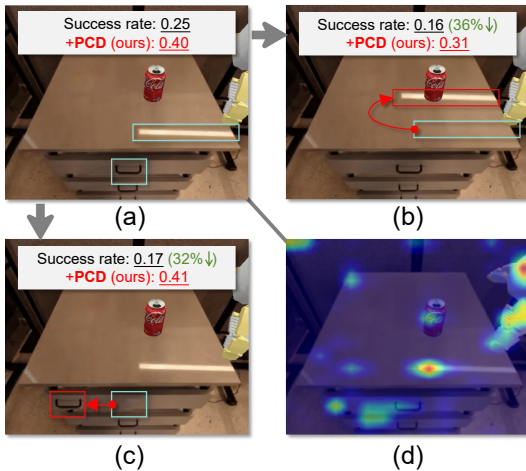


Figure 1: **Robot policies tend to spuriously correlate task-irrelevant features with actions, compromising their ability to generalize to unseen scenarios.** As observed, changing the light position from (a) to (b) and the drawer handle position from (a) to (c) results in 36% and 32% drops in the performance of the baseline policy OpenVLA [20], respectively. More results are in **Appendix A.1**.

across 15 manipulation tasks on multiple robotic platforms. We believe that our PCD provides a novel perspective for achieving robust adaptation of robot policies to downstream tasks.

2 Related Work

Robotic Foundation Models. The rapid development of robotic foundation models or generalist robot policies has been significantly inspired by the success of large visual and language models [18, 52, 42].

To the best of our knowledge, this is the first work to introduce a training-free approach for resolving the spurious correlation issue in robot policies. We conduct extensive evaluations in both simulation and real-world environments, across a total of 15 diverse tasks, and on top of three open-source robot policies—including the autoregressive policy OpenVLA [20] and the diffusion-based policies Octo [32] and π_0 [3]. The achieved results demonstrate the strong flexibility and effectiveness of our PCD approach. On simulation benchmarks, PCD enhances the performance of Octo, OpenVLA and π_0 by 31%, 41% and 8%, respectively. On real-world manipulation tasks, PCD outperforms the state-of-the-art robot policy π_0 by 108%.

Contributions. Our contributions in this work are threefold. **1)** We propose PCD, a simple, training-free, and easy-to-implement scheme to tackle the spurious correlation issue of robot policies. **2)** PCD can be used as a plugin to enhance both autoregressive and diffusion-based policies, without requiring fine-tuning or access to pre-trained model weights. **3)** Extensive experiments demonstrate the flexibility and effectiveness of PCD, consistently improving performance over three state-of-the-art robot policies

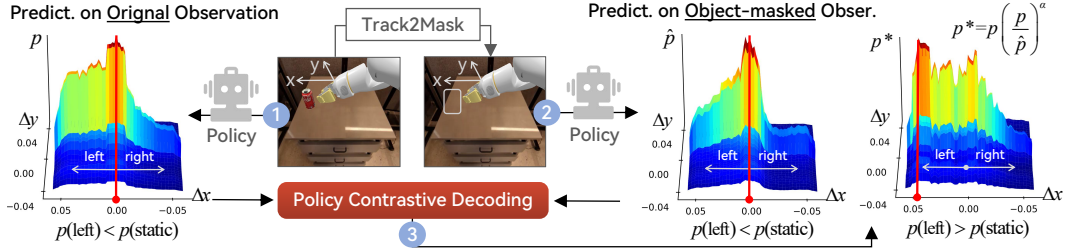


Figure 2: **Overview of our Proposed Policy Contrastive Decoding (PCD) approach.** PCD serves as a *plugin* to redirect the robot policy’s focus toward object-relevant visual cues by contrasting action probability distributions derived from original observations p and object-masked observations \hat{p} . For illustrative purposes, we visualize the predictions only in the Δx and Δy dimensions of the robot action space $[\Delta x, \Delta y, \Delta z, \text{rot}_x, \text{rot}_y, \text{rot}_z, \text{gripper}]$.

Robot policies can be categorized based on action prediction strategies into autoregressive models and diffusion-based policies. Autoregressive policies sequentially generate action tokens based on previous outputs [4, 5, 9, 50, 1, 53, 54]. OpenVLA [20] equips with a Llama 2 [42] language model alongside a visual encoder that merges pretrained features from SigLIP [52] and DINO-v2 [34]. Diffusion-based policies simultaneously generate entire action dimensions by performing diffusion processes on noise [32, 27]. Octo [40] learns a lightweight policy on the OXE dataset [9], enabling rapid adaptation to unknown tasks and scenarios on standard consumer-grade GPUs. π_0 [3] exhibits flexible control over different robot types by leveraging pre-trained general knowledge from vision-language models. Although most robot policies are trained on extensive robotic behavior datasets, recent studies have shown that slight variations in deployment scenarios can significantly affect their generalization performance on downstream tasks in real-world environments [11, 12, 29].

Contrastive Decoding. Recent studies in large vision-language models (VLMs) have highlighted the challenge of *hallucination* [14, 37, 26], where models generate inaccurate or misleading outputs not grounded in the input data. Contrastive Decoding (CD) [10, 7, 22] suppresses hallucinations by comparing output distributions from original and distorted input without altering the model’s weights. Instruction Contrastive Decoding (ICD) [46] is used to combat hallucinations in multimodal tasks by modulating the confidence in multimodal alignment of the model’s visual and textual inputs, enabling it to distinguish between hallucinated and relevant tokens. Visual Contrastive Decoding (VCD) [35, 10] aims to reduce object hallucinations by comparing outputs from original and distorted visual inputs. This approach provides a computationally efficient solution as it requires neither additional training nor external pre-trained models. Our proposed Policy Contrastive Decoding (PCD) approach in this work is mainly inspired by the success of VCD schemes. However, unlike those schemes that contrast output distributions from original and noise-distorted [35] or image-removed [10] inputs to counteract LVLMs’ overreliance on language priors, our PCD contrasts action probability distributions derived from original and object-masked inputs, thereby redirecting the robot policy’s focus to object-relevant visual features and enhancing their generalization across different scenarios.

3 Proposed Approach

In this section, we present PCD, our training-free, plug-and-play scheme designed to tackle the spurious correlation issue for existing generalist robot policies. Notably, PCD does not require access to the pre-trained parameters of these robot policies; i.e., it treats each robot policy as a *black-box*.

3.1 Preliminaries

This work focuses on robot manipulation tasks where the objective is to leverage a learned language-conditioned policy $\pi_\theta(\mathbf{a}_i \mid \mathbf{o}_i, \ell)$ to predict an M -dimensional action $\mathbf{a}_i = [a_1, \dots, a_M] \in \mathbb{R}^M$ conditioned on the current visual observation \mathbf{o}_i and the language instruction ℓ of the task. In this part, we formalize two mainstream paradigms for action prediction: autoregressive action prediction (e.g., OpenVLA [20]) and diffusion-based action prediction (e.g., Octo [32] and π_0 [3]).

Autoregressive Robot Policies. The policy decomposes the action prediction task into sequential token generation. Each action dimension a_t of \mathbf{a}_i is sampled autoregressively from the probability distribution, conditioned on the visual observation \mathbf{o}_i , the language instruction ℓ , as well as the previously predicted dimensions $a_{<t} = \{a_t\}_{t=1}^{t-1}$:

$$a_t \sim \pi_\theta(a_t | \ell, \mathbf{o}_i, a_{<t}).$$

For example, OpenVLA first encodes \mathbf{o}_i through a hybrid vision backbone (DINOv2 [6] w/ SigLIP [51]) and tokenizes ℓ using a pre-trained language model (Llama 2 [43]). These multimodal features are fused in the LLM’s embedding space, which then autoregressively emits M discrete tokens. Each token is finally mapped to an action dimension a_t via a de-tokenizer [20].

Diffusion-based Robot Policies. The policy frames action generation as an iterative denoising process [15]. Denote \mathbf{e}_i the multimodal embeddings fusing \mathbf{o}_i and ℓ . Starting from Gaussian noise $\mathbf{a}_i^K \sim \mathcal{N}(\mathbf{0}, \mathbf{I})$, the reverse diffusion process refines all the M dimensions of the action \mathbf{a}_i in parallel over K steps through:

$$\mathbf{a}_i^{k-1} = \alpha(\mathbf{a}_i^k - \gamma \epsilon_\theta(\mathbf{a}_i^k, \mathbf{e}_i, k)) + \mathcal{N}(\mathbf{0}, \sigma^2 \mathbf{I}) \quad (1)$$

where \mathbf{a}_i^k is the noisy action at diffusion step k , $\epsilon_\theta(\mathbf{a}_i^k, \mathbf{e}_i, k)$ is the denoising network, and α, γ, σ are parameters of a cosine noise schedule [33]. By jointly optimizing the entire M action dimensions of \mathbf{a}_i , diffusion-based robot policies enable fine-grained sampling from the joint probability $\pi_\theta(\mathbf{a}_i | \ell, \mathbf{o}_i)$ of all action dimensions.

3.2 Policy Contrastive Decoding (PCD)

The core idea of our proposed PCD method is to eliminate the adverse effect of spurious correlations by redirecting the robot policy’s focus toward object-relevant features during inference. To facilitate the introduction of our PCD, we define spurious correlations as follows.

Definition 3.1 (Spurious Correlations): Let observations \mathbf{o} and language instructions l be generated by a set of L underlying latent factors $\{c_j\}_{j=1}^L$. These factors are decomposed into task-relevant factors, denoted by the random variable \mathbf{u} , which exclusively determine the ground-truth expert policy such that $p(\mathbf{a} | \mathbf{o}, l) = p(\mathbf{a} | \mathbf{u})$, and task-irrelevant factors, denoted by the random variable \mathbf{v} , which have no causal effect on the expert’s actions \mathbf{a} . Spurious correlation is then defined as the statistical dependence between the action \mathbf{a} and these task-irrelevant factors \mathbf{v} observed under the training distribution $p_{\text{train}}(\mathbf{a}, \mathbf{v})$, quantified by the mutual information $I_{\text{train}}(\mathbf{a}, \mathbf{v})$.

Spurious correlations, indicated by mutual information $I_{\text{train}}(\mathbf{a}, \mathbf{v}) > 0$ in the training set, allow a robot policy π_θ to infer action \mathbf{a} from task-irrelevant factors \mathbf{v} . These factors act as shortcuts. However, such correlations are unreliable. Under *out-of-distribution* (OOD) conditions—stemming from environmental shifts or compounding robotic errors— \mathbf{v} may change independently of task-relevant factors \mathbf{u} and, consequently, \mathbf{a} , leading to inaccurate action predictions.

A direct approach to mitigate learning from spurious correlations involves filtering out \mathbf{v} and utilizing only \mathbf{u} . Nevertheless, identifying and neutralizing spurious features is challenging due to their significant variability across tasks and scenarios, coupled with interdependencies within the feature space. Drawing inspiration from Vision Contrastive Decoding (VCD) [35, 10], which effectively reduces hallucinations in vision-language models, we introduce Policy Contrastive Decoding (PCD). PCD aims to shift the robot policy’s focus from spurious features \mathbf{v} towards task-relevant features \mathbf{u} associated with the target object. This is achieved by contrasting model outputs derived from original visual inputs with those from object-masked visual inputs.

Method Overview. Fig. 2 presents an overview of our PCD approach. Suppose we have a pretrained policy π_θ . Given the current visual observation \mathbf{o}_i and the language command ℓ , we first generate two distinct action probability distributions of \mathbf{a}_i : one is $\pi_\theta(\mathbf{a}_i | \ell, \mathbf{o}_i)$ conditioned on the *original* visual input \mathbf{o}_i , and the other is $\pi_\theta(\mathbf{a}_i | \ell, \hat{\mathbf{o}}_i)$ conditioned on *object-masked* counterpart $\hat{\mathbf{o}}_i$ that removes all task-relevant factors related to target objects. Then, a new contrastive action probability distribution $\pi_\theta^*(\mathbf{a}_i | \ell, \mathbf{o}_i)$ is obtained by contrasting $\pi_\theta(\mathbf{a}_i | \ell, \mathbf{o}_i)$ and $\pi_\theta(\mathbf{a}_i | \ell, \hat{\mathbf{o}}_i)$:

$$\pi_\theta^*(\mathbf{a}_i | \ell, \mathbf{o}_i) = \frac{1}{C} \cdot \pi_\theta(\mathbf{a}_i | \ell, \mathbf{o}_i) \left(\frac{\pi_\theta(\mathbf{a}_i | \ell, \mathbf{o}_i)}{\pi_\theta(\mathbf{a}_i | \ell, \hat{\mathbf{o}}_i)} \right)^\alpha, \quad (2)$$

where C is a normalization constant and a larger value of $\alpha \geq 0$ indicates a stronger amplification of differences between the two distributions. Particularly, $\alpha = 0$ recovers the baseline policy. In such a manner, the obtained p_t^* amplifies model predictions on object-relevant features in \mathbf{u} , thus exhibiting insensitivity to spurious features in \mathbf{v} , as illustrated in Fig. 2.

To guarantee the flexibility and practical applicability of our PCD method, we need to address the following two questions:

- 1) How can object-masked observations $\hat{\mathbf{o}}_i$ be automatically generated for each trajectory?
- 2) How can we approximate the policy distribution π_θ for diffusion-based policies?

Tracking-to-Mask. We overcome the first question by devising a *Tracking-to-Mask (Track2Mask)* strategy, which enables precise object masking for sequential visual observations along each trajectory, requiring minimal or no human intervention. Concretely, the first step of Track2Mask is to annotate the task-specified objects in the *initial* visual observation. Inspired by visual prompting techniques [45, 56], one can annotate the target objects in the initial observation using Point or Box prompts. Besides, we provide the option of leveraging off-the-shelf (open vocabulary) object detection models, such as Grounding DINO [28] for automatic object annotation. Next, the SAM2 [21] model is employed to track and segment the target object across subsequent observations in the trajectory, and the segmented objects are then inpainted to obtain object-masked observations. For more details of Track2Mask, please refer to **Appendix A.2**.

KDE-based Probabilistic Modeling. We address the second question using *KDE-based Probabilistic Modeling (KDE-PM)*, which approximates action probability distributions for diffusion-based policies through kernel density estimation (KDE) [47]. Specifically, we first use the pretrained diffusion-based policy to sample N candidate action predictions: $\{\mathbf{a}_i(j)\}_{j=1}^N$, where $\mathbf{a}_i(j) = [a_1(j), \dots, a_M(j)] \sim \pi_\theta(\mathbf{a}_i|l, \mathbf{o}_i)$. With the assumption that all action dimensions are independent, i.e., $\pi_\theta(\mathbf{a}_i|l, \mathbf{o}_i) = \prod_{t=1}^M \pi_\theta(a_t|l, \mathbf{o}_i)$, we calculate an approximated probability distribution for each action dimension of the action \mathbf{a}_i via KDE:

$$\pi_\theta(a_t|l, \mathbf{o}_i) \approx \frac{1}{C'} \sum_{j=1}^N \mathcal{K}\left(\frac{a_t - a_t(j)}{b}\right), \quad t = 1, \dots, M, \quad (3)$$

where C' is a normalization constant and $\mathcal{K}(\cdot)$ indicates a Gaussian kernel $\mathcal{K}(u) = \frac{1}{\sqrt{2\pi}} e^{-\frac{u^2}{2}}$, b is the bandwidth parameter controlling the smoothness of the distribution, and $\{a_t(j)\}_{j=1}^N$ are the N candidate actions for the t -th dimension of the action \mathbf{a}_i , generated from the diffusion process. Similarly, we can derive an action probability distribution for a_t conditioned on object-masked $\hat{\mathbf{o}}_i$, i.e., $\pi_\theta(a_t|l, \hat{\mathbf{o}}_i)$. With the independence assumption, from $\pi_\theta(a_t|l, \mathbf{o}_i)$ and $\pi_\theta(a_t|l, \hat{\mathbf{o}}_i)$ we can compute the joint action distributions, which are then used to compute the contrastive action probability $\pi_\theta^*(\mathbf{a}_i|l, \mathbf{o}_i)$ using Eq. (2). In this way, our PCD is compatible with diffusion-based robot policies.

Inference with PCD. As a *training-free* method, our proposed PCD can be employed as a plugin to improve the inference stage of different types of robot policies (i.e., autoregressive policies and diffusion-based policies). Specifically, for a pre-trained robot policy $\pi_\theta(\mathbf{a}_i | \mathbf{o}_i, \ell)$, given the current observation \mathbf{o}_i , we can obtain the object-masked $\hat{\mathbf{o}}_i$ (i.e., $\hat{\mathbf{o}}_i$) leveraging the devised Track2Mask strategy. Based on \mathbf{o}_i , $\hat{\mathbf{o}}_i$ and a language command ℓ , the autoregressive policy directly computes contrastive action probability distributions for deriving \mathbf{a}_i (w/ Eq. (2)), whereas the diffusion-based policy requires performing the KDE-PM process on its output predictions to achieve the same goal. Pseudocode for our PCD method is provided in **Algorithm 1**.

4 Experiments

In this section, we seek to answer the following questions:

- 1) Can PCD improve robot policies in both simulation and real-world environments?
- 2) How does the performance vary with different design choices?
- 3) What kinds of spurious correlations can our PCD tackle?

Algorithm 1 PCD: Policy Contrastive Decoding

Require: A pre-trained robot policy: $\pi_\theta(\mathbf{a}_i | \mathbf{o}_i, \ell)$; initial observation \mathbf{o}_0 ; language command ℓ ; maximum time step S .

- 1: $s \leftarrow 0$
 - 2: **while** $s \leq S$ **do**
 - 3: Obtain object-masked $\mathbf{o}_s: \hat{\mathbf{o}}_s$ ▷ w/ Track2Mask
 - 4: Obtain $\pi_\theta(\mathbf{a}_s | l, \mathbf{o}_s)$ and $\pi_\theta(\mathbf{a}_s | l, \hat{\mathbf{o}}_s)$ ▷ w/ KDE-PM for diffusion-based policies
 - 5: Compute $\pi_\theta^*(\mathbf{a}_s | l, \mathbf{o}_s)$ using Eq. (2)
 - 6: Sample \mathbf{a}_s from $\pi_\theta^*(\mathbf{a}_s | l, \mathbf{o}_s)$ and execute \mathbf{a}_s
 - 7: $\mathbf{o}_{s+1} \leftarrow$ New observation ▷ Obtain a new observation
 - 8: $s \leftarrow s + 1$
 - 9: **end while**
-

Table 1: **SIMPLER Performance**—Success rates of the autoaggressive policy OpenVLA [20] and the diffusion-based policies Octo [32] and π_0 [3] integrated w/ or w/o PCD on 9 tasks from Google Robot and WidowX. Task-specific objects in the initial observation are annotated by artificial Point and Box prompts or the automatic detection results of Grounding DINO [28]. **As a plug-and-play approach, PCD consistently enhances the three policies by large margins over the 9 tasks.**

Tasks	OpenVLA[20]				Octo [32]				π_0 [3]				
	Base	+PCD			Base	+PCD			Base	+PCD			
		Point	Box	GDINO		Point	Box	GDINO		Point	Box	GDINO	
Average	0.17	0.24	0.21	0.24	0.16	0.21	0.20	0.19	0.65	0.70	0.69	0.69	
		+41%	+24%	+41%		+31%	+25%	+19%		+8%	+6%	+6%	
Google Robot	Close Drawer	0.41	0.68	0.66	0.77	0.33	0.28	0.38	0.16	0.75	0.72	0.76	0.71
	Move Near	0.58	0.62	0.52	0.53	0.07	0.13	0.12	0.13	0.73	0.74	0.71	0.75
	Open Drawer	0.20	0.29	0.29	0.26	0.00	0.01	0.00	0.02	0.39	0.49	0.50	0.52
	Pick Coke Can	0.25	0.40	0.42	0.42	0.28	0.54	0.49	0.52	0.84	0.88	0.87	0.87
	Apple Drawer	0.00	0.00	0.00	0.00	0.00	0.00	0.00	0.00	0.11	0.29	0.24	0.22
WidowX.	Carrot Plate	0.00	0.08	0.00	0.04	0.14	0.28	0.22	0.19	0.59	0.67	0.62	0.62
	Eggplant Basket	0.01	0.02	0.02	0.11	0.48	0.41	0.38	0.44	0.93	0.86	0.87	0.88
	Spoon Towel	0.00	0.02	0.00	0.03	0.10	0.15	0.14	0.15	0.83	0.89	0.88	0.86
	Stack Cube	0.04	0.01	0.00	0.00	0.00	0.05	0.06	0.07	0.67	0.77	0.78	0.75

We answer the first question in Sections 4.1 and 4.2, the second question in Section 4.3, and the third question in Section 4.4. Detailed descriptions of the baseline robot policies and the evaluation tasks used in simulation and real-world environments are presented in **Appendix A.3**.

4.1 Simulation Experiments

We perform simulation experiments in SIMPLER [24], a real-to-sim evaluation environment designed specifically for real-robot policies. SIMPLER accurately reflects real-world performance, enabling reliable assessment of robotic policies. We evaluate 9 tasks across two robot platforms: 5 tasks using the Google Robot and 4 tasks using the WidowX arm.

Experimental Setup. We conduct experiments on top of three diverse robot policies, including the autoregressive policy OpenVLA [20], and the diffusion-based policies Octo (base) [32] and π_0 [3]. We treat these policies as black-boxes, applying PCD solely based on the output action probability distributions for OpenVLA and the output actions for Octo and π_0 . For our PCD, we annotate the target object in the initial observation using three manners: artificial Point and Box prompts, and automatic detection results from Grounding DINO [28]. The number of the sampled noise vectors N in KDE-PM is set to 24 for Octo and π_0 . We perform ablation studies on the hyperparameter α in Eq. (2), as well as on the object detection strategies and object inpainting paradigms of the devised Track2Mask module in Section 4.3.

Results and Analysis. Table 1 reports the performance of three robot policies (i.e., OpenVLA [20], Octo [32] and π_0 [3]) integrated w/ or w/o our PCD across a total of 9 tasks from Google Robot and WidowX. From the results in the table, we have the following key observations. **1)** Our PCD consistently improves the three baseline policies over the 9 tasks from both the Google Robot and

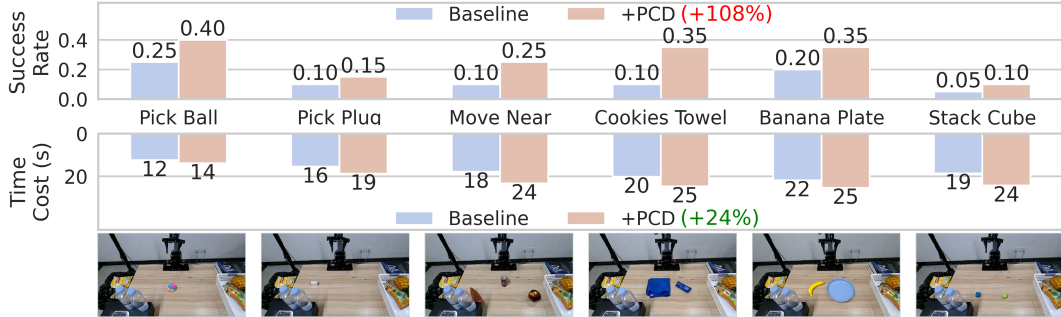


Figure 3: **Real-world Performance**—Success rates and time costs of the state-of-the-art robot policy π_0 [3] integrated w/ or w/o PCD on 6 real-world tasks. The target objects in the initial observation are automatically annotated by Grounding DINO [28]. **PCD delivers a remarkable 108% performance improvement on the baseline policy, though it incurs a 24% increase in time cost.**

WidowX robotic platforms. On average, PCD boosts the success rates of the autoregressive policy OpenVLA, and the diffusion-based policies Octo and π_0 by up to **41%**, **31%** and **8%**, respectively. **2)** Our PCD exhibits stable and outstanding performance across the three object annotation strategies, including artificial Point and Box prompts and automatic object detection with Grounding DINO, underscoring its effectiveness and adaptability. In particular, on the Octo and OpenVLA baseline policies, leveraging the off-the-shelf model Grounding DINO demonstrates better performance than using human Point and Box prompts, while showing comparable results on π_0 , highlighting the practical applicability of the PCD method. **3)** Compared to OpenVLA and Octo, the baseline model π_0 demonstrates significantly superior performance across all 9 tasks. For instance, OpenVLA and Octo achieve near-zero success rates on both “Apple Drawer” and “Stack Cube” tasks whereas π_0 achieve success rates of **11%** and **67%** on these two tasks, respectively. Despite this, from the average results over the 9 tasks, our PCD still enhances the strong baseline π_0 by **8%**. In summary, the obtained results in the table demonstrate that our PCD approach can be used as a plugin to improve different types of robot policies.

4.2 Real-world Experiments

In this section, we conduct experiments on real-world tasks to assess PCD’s practical effectiveness.

Experimental Setup. The simulation experiments show that π_0 significantly outperforms Octo and OpenVLA. Therefore, we employ π_0 as the baseline policy to validate the effectiveness of our PCD approach, as shown in Fig. 3. Considering the generalization limitations of existing robot policies in real-world environments, we first finetune π_0 on downstream real-world tasks before evaluating PCD’s performance. We design 6 manipulation tasks that focus on evaluating the policy’s performance along multiple dimensions: spatial reasoning and interacting with various objects and scenes. The π_0 policy is jointly fine-tuned on the 6 real-world tasks, with each task consisting of 10 training demonstrations. During inference, we conduct 20 trials for each real-world task and randomize the configurations and orientations of task-specific objects for each trial. We use an AGILEX PIPER 6DOF robot arm in our experiments. For our PCD, we leverage the off-the-shelf model Grounding DINO to detect task-specific objects in the initial observation, and use LaMa [39] to inpaint those objects segmented by the SAM2 [21] model. All other hyperparameters are kept consistent with the settings applied in the simulation experiments.

Results and Analysis. Fig. 3 reports the success rates as well as time costs of the state-of-the-art robot policy π_0 [3] integrated w/ or w/o our PCD on 6 real-world tasks. For each task, we record the time cost (in seconds) from the start of the inference process to the successful completion of the task. From the obtained results in the figure, we have several key observations. **1)** PCD consistently improves the success rates of the strong baseline policy across six real-world tasks, achieving an average enhancement of **108%**. **2)** While PCD significantly boosts success rates, it also increases the time cost by 24% on average compared to the baseline policy. However, considering the notable improvement in task completion success rates, this trade-off is acceptable in a wide range of real-world robotic applications. **3)** PCD demonstrates consistent performance improvements across tasks of varying complexity. For example, in the challenging “Stack Cube” task, PCD improves the

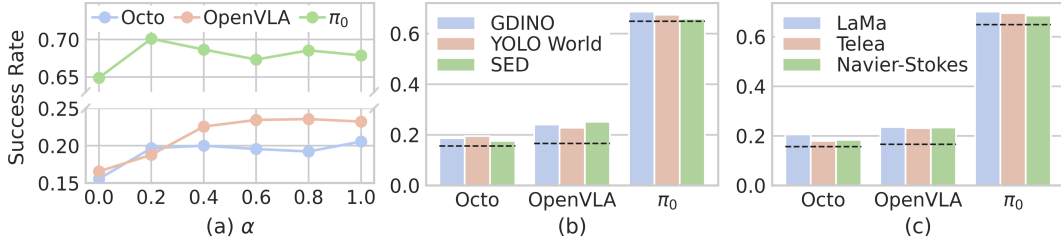


Figure 4: Ablation studies on (a) the hyperparameter α in Eq. (2), (b) the object detection schemes and (c) object inpainting strategies in Track2Mask. $\alpha = 0$ in (a) and the black dotted lines in (b)(c) represent the performance of the baseline policies. The results are averaged over the 9 simulation tasks. **PCD consistently improves the three policies when $\alpha > 0$ and exhibits low sensitivity to changes in off-the-shelf object detection and inpainting strategies.**

success rate from 0.05 to 0.10, showing its strong adaptability and robustness across diverse scenarios. Additionally, the backgrounds of these six real-world tasks are far more complex than those of the nine simulation tasks, containing numerous distracting elements such as plastic bottles, baskets, and trash cans. Nevertheless, our PCD shows remarkable advantages. It is worth mentioning that we use consistent PCD hyperparameters across tasks in both the simulation and real-world environments, without carefully tuning task-specific PCD hyperparameters (e.g., α) for each individual task, leaving room for potential performance improvements through task-specific parameter tuning.

4.3 Ablation Studies

In this section, we conduct ablation studies to explore how the performance of our PCD varies with different design decisions. We perform experiments in the SIMPLER simulation environment, and report the average results across the nine tasks for our PCD applied to the three baseline policies.

Effect of α . As formulated in Eq. (2), PCD leverages the hyperparameter α to control the level of amplification between output distributions from original and object-masked visual inputs. A larger α value indicates a stronger amplification of differences between the two distributions, while $\alpha = 0$ reduces to regular prediction. We adjust α by setting it to $\{0, 0.2, 0.4, 0.6, 0.8, 1.0\}$, and report the performance of our PCD method over the 9 tasks in Fig. 4 (a). $\alpha = 0$ represents the baseline policies. As can be observed, our PCD consistently improves Octo, OpenVLA and π_0 when $\alpha > 0$, demonstrating its effectiveness and stability. Particularly, PCD yields the best results on Octo, OpenVLA and π_0 when the values of α are set to 1.0, 0.8, and 0.2, respectively.

Effect of Off-the-shelf Object Detection Models. Beyond leveraging artificial Point and Box prompts, the devised Track2Mask module can employ off-the-shelf open vocabulary object detection models to annotate task-specific objects in the initial observation of the trajectory during inference. Fig. 4 (b) presents an ablation study on various automatic object detection models, including the Grounding DINO [28] model discussed in the main paper, as well as the open vocabulary object detection model YOLO World [8] and semantic segmentation model SED [48]. The output of these models is fed into the SAM2 [21] model for tracking and segmenting the detected objects across subsequent observations in the trajectory. As can be seen, our PCD consistently improves the baseline policies when integrated with each of the three off-the-shelf models, showcasing its effectiveness and stability. Generally, the Grounding DINO model yields the best results among the three models.

Effect of Object Inpainting Strategies. Once the objects specified in the language instruction of the target task are segmented by the SAM2 model, they are inpainted to create object-masked observations. In this experiment, we investigate the effect of different object inpainting strategies on PCD’s performance. Fig. 4 (c) shows the results of PCD integrated with three inpainting strategies: Telea [41] and Navier-Stokes [2] and LaMa [39]. As indicated in the figure, our PCD approach consistently improves the baseline policies across all strategies, showcasing its effectiveness and stability. Furthermore, PCD demonstrates low sensitivity to variations in the three object inpainting strategies, further validating its applicability and robustness. Notably, LaMa delivers the best results across all three baseline policies.

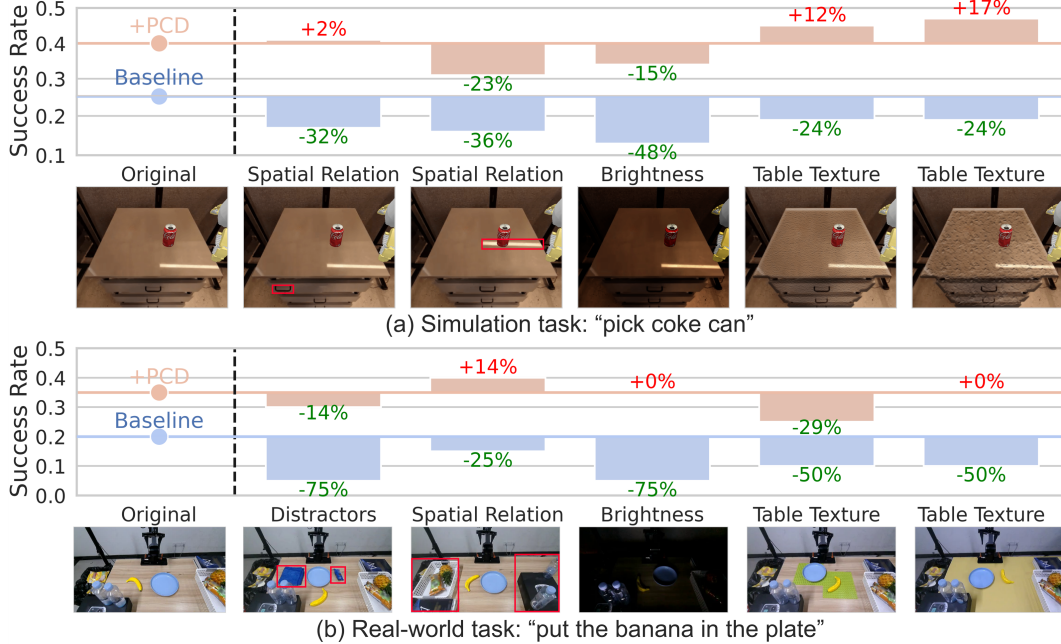


Figure 5: Performance of baseline policies integrated w/ or w/o our proposed PCD approach in unseen testing scenarios. OpenVLA [20] and π_0 [3] are used as baselines in simulation and real-world environments, respectively. **PCD effectively mitigates the side effects of various types of spurious correlations, boosting the robot policy’s generalization to novel scenarios.**

4.4 Robustness to Various Kinds of Spurious Correlations

The central concept of our proposed PCD approach in this work is to overcome the adverse effects of spurious features on the decision-making of robot policies. It is crucial to investigate the following question: What types of spurious correlations can our PCD effectively address? To this end, we evaluate the performance of the OpenVLA [20] and π_0 [3] policies across a range of scenario variations in both simulation and real-world environments, including changes in spatial relationships, brightness, distractors, and table textures in visual observations, as illustrated in Fig. 5. The results shown in the figure lead to the following observations. **1)** Consistent with the previous experimental results, our PCD significantly improves the performance of the baseline policies on both simulation and real-world tasks. **2)** Both baseline policies experience substantial drops in performance when testing scenarios are modified. For example, altering the brightness of visual observations results in **48%** and **75%** decreases in success rates for the two policies, respectively. **3)** Our proposed PCD approach consistently alleviates the performance degradation of the baseline policies across all unseen testing scenarios. Remarkably, after integrating PCD, the two baseline policies even performs better in **4/10** of unseen scenarios than in the original training scenarios. In summary, the results in the figure reveal that robot policies often form spurious correlations between task-irrelevant features and actions, limiting their generalization capacity beyond the training data distribution. Our proposed PCD approach can serve as a plugin to mitigate the adverse effects of various types of spurious correlations on the generalization of robot policies.

5 Conclusion, Limitations and Future Work

In this work, propose Policy Contrastive Decoding (PCD) to tackle the adverse effects of spurious correlations learned by generalist robot policies. PCD redirects the policy’s attention from spurious features to object-relevant ones during inference by contrasting action probability distributions obtained from original and object-masked inputs. As a *plug-and-play* approach, PCD can enhance both autoregressive and diffusion-based policies, without requiring fine-tuning or access to pre-trained model weights. Comprehensive experiments demonstrate PCD’s flexibility and effectiveness,

achieving consistent improvements over three state-of-the-art robot policies across a total of 15 tasks in simulation and real-world environments.

While our PCD demonstrates effectiveness and flexibility, there are certain limitations. **1)** PCD performs object detection and segmentation for each visual observation in the trajectory to produce object-masked observations, which increases the computational overhead of the baseline police. Recent progress in fast LLM inference techniques [55, 23, 30] could potentially enhance the computational efficiency of our PCD approach. **2)** This work concentrates exclusively on addressing the spurious correlation issue in robot policies during the testing stage, without exploring methods to prevent the learning of such correlations during training. Hence, future work will focus on investigating effective strategies to tackle spurious correlations at both the training and inference levels.

References

- [1] S. Belkhale, T. Ding, T. Xiao, P. Sermanet, Q. Vuong, J. Tompson, Y. Chebotar, D. Dwibedi, and D. Sadigh. Rt-h: Action hierarchies using language. *arXiv preprint arXiv:2403.01823*, 2024.
- [2] M. Bertalmio, A. L. Bertozzi, and G. Sapiro. Navier-stokes, fluid dynamics, and image and video inpainting. In *CVPR*, volume 1. IEEE, 2001.
- [3] K. Black, N. Brown, D. Driess, et al. Pi-0: A vision-language-action flow model for general robot control. *arXiv preprint arXiv:2410.24164*, 2024.
- [4] A. Brohan, N. Brown, J. Carbajal, et al. Rt-1: Robotics transformer for real-world control at scale. *arXiv preprint arXiv:2212.06817*, 2022.
- [5] A. Brohan, N. Brown, J. Carbajal, et al. Rt-2: Vision-language-action models transfer web knowledge to robotic control. *arXiv preprint arXiv:2307.15818*, 2023.
- [6] M. Caron, H. Touvron, I. Misra, H. Jégou, J. Mairal, P. Bojanowski, and A. Joulin. Dinov2: Learning robust visual features without supervision. *arXiv preprint arXiv:2304.07193*, 2023.
- [7] Z. Chen, Z. Zhao, H. Luo, H. Yao, B. Li, and J. Zhou. Halc: Object hallucination reduction via adaptive focal-contrast decoding. *arXiv preprint arXiv:2403.00425*, 2024.
- [8] T. Cheng, L. Song, Y. Ge, W. Liu, X. Wang, and Y. Shan. Yolo-world: Real-time open-vocabulary object detection. In *CVPR*, 2024.
- [9] E. Collaboration, A. O’Neill, A. Rehman, A. Gupta, A. Maddukuri, A. Gupta, A. Padalkar, A. Lee, A. Pooley, A. Gupta, A. Mandlekar, A. Jain, A. Tung, A. Bewley, A. Herzog, A. Irgan, A. Khazatsky, A. Rai, A. Gupta, A. Wang, A. Kolobov, A. Singh, A. Garg, A. Kembhavi, A. Xie, A. Brohan, A. Raffin, A. Sharma, A. Yavary, A. Jain, A. Balakrishna, A. Wahid, B. Burgess-Limerick, B. Kim, B. Schölkopf, B. Wulfe, B. Ichter, C. Lu, C. Xu, C. Le, C. Finn, C. Wang, C. Xu, C. Chi, C. Huang, C. Chan, C. Agia, C. Pan, C. Fu, C. Devin, D. Xu, D. Morton, D. Driess, D. Chen, D. Pathak, D. Shah, D. Büchler, D. Jayaraman, D. Kalashnikov, D. Sadigh, E. Johns, E. Foster, F. Liu, F. Ceola, F. Xia, F. Zhao, F. V. Fruejri, F. Stulp, G. Zhou, G. S. Sukhatme, G. Salhotra, G. Yan, G. Feng, G. Schiavi, G. Berseth, G. Kahn, G. Yang, G. Wang, H. Su, H.-S. Fang, H. Shi, H. Bao, H. B. Amor, H. I. Christensen, H. Furuta, H. Bharadhwaj, H. Walke, H. Fang, H. Ha, I. Mordatch, I. Radosavovic, I. Leal, J. Liang, J. Abou-Chakra, J. Kim, J. Drake, J. Peters, J. Schneider, J. Hsu, J. Vakil, J. Bohg, J. Bingham, J. Wu, J. Gao, J. Hu, J. Wu, J. Wu, J. Sun, J. Luo, J. Gu, J. Tan, J. Oh, J. Wu, J. Lu, J. Yang, J. Malik, J. Silvério, J. Hejna, J. Booher, J. Tompson, J. Yang, J. Salvador, J. J. Lim, J. Han, K. Wang, K. Rao, K. Pertsch, K. Hausman, K. Go, K. Gopalakrishnan, K. Goldberg, K. Byrne, K. Oslund, K. Kawaharazuka, K. Black, K. Lin, K. Zhang, K. Ehsani, K. Lekkala, K. Ellis, K. Rana, K. Srinivasan, K. Fang, K. P. Singh, K.-H. Zeng, K. Hatch, K. Hsu, L. Itti, L. Y. Chen, L. Pinto, L. Fei-Fei, L. Tan, L. J. Fan, L. Ott, L. Lee, L. Weihs, M. Chen, M. Lepert, M. Memmel, M. Tomizuka, M. Itkina, M. G. Castro, M. Spero, M. Du, M. Ahn, M. C. Yip, M. Zhang, M. Ding, M. Heo, M. K. Srirama, M. Sharma, M. J. Kim, N. Kanazawa, N. Hansen, N. Heess, N. J. Joshi, N. Suenderhauf, N. Liu, N. D. Palo, N. M. M. Shafiqullah, O. Mees, O. Kroemer, O. Bastani, P. R. Sanketi, P. T. Miller, P. Yin, P. Wohlhart, P. Xu, P. D. Fagan, P. Mitrano, P. Sermanet, P. Abbeel, P. Sundaresan, Q. Chen, Q. Vuong, R. Rafailov, R. Tian, R. Doshi, R. Mart’ in-Mart’ in, R. Bajjal, R. Scalise, R. Hendrix, R. Lin, R. Qian, R. Zhang, R. Mendonca, R. Shah, R. Hoque, R. Julian, S. Bustamante, S. Kirmani, S. Levine, S. Lin, S. Moore, S. Bahl,

- S. Dass, S. Sonawani, S. Tulsiani, S. Song, S. Xu, S. Haldar, S. Karamcheti, S. Adebola, S. Guist, S. Nasiriany, S. Schaal, S. Welker, S. Tian, S. Ramamoorthy, S. Dasari, S. Belkhale, S. Park, S. Nair, S. Mirchandani, T. Osa, T. Gupta, T. Harada, T. Matsushima, T. Xiao, T. Kollar, T. Yu, T. Ding, T. Davchev, T. Z. Zhao, T. Armstrong, T. Darrell, T. Chung, V. Jain, V. Kumar, V. Vanhoucke, W. Zhan, W. Zhou, W. Burgard, X. Chen, X. Chen, X. Wang, X. Zhu, X. Geng, X. Liu, X. Liangwei, X. Li, Y. Pang, Y. Lu, Y. J. Ma, Y. Kim, Y. Chebotar, Y. Zhou, Y. Zhu, Y. Wu, Y. Xu, Y. Wang, Y. Bisk, Y. Dou, Y. Cho, Y. Lee, Y. Cui, Y. Cao, Y.-H. Wu, Y. Tang, Y. Zhu, Y. Zhang, Y. Jiang, Y. Li, Y. Li, Y. Iwasawa, Y. Matsuo, Z. Ma, Z. Xu, Z. J. Cui, Z. Zhang, Z. Fu, and Z. Lin. Open x-embodiment: Robotic learning datasets and rt-x models. *arXiv preprint arXiv:2310.08864*, 2024.
- [10] A. Favero, L. Zancato, M. Trager, S. Choudhary, P. Perera, A. Achille, A. Swaminathan, and S. Soatto. Multi-modal hallucination control by visual information grounding. In *CVPR*, pages 14303–14312, 2024.
- [11] R. Firoozi, J. Tucker, S. Tian, A. Majumdar, J. Sun, W. Liu, Y. Zhu, S. Song, A. Kapoor, K. Hausman, et al. Foundation models in robotics: Applications, challenges, and the future. *The International Journal of Robotics Research*, page 02783649241281508, 2023.
- [12] J. Gao, B. Sarkar, F. Xia, T. Xiao, J. Wu, B. Ichter, A. Majumdar, and D. Sadigh. Physically grounded vision-language models for robotic manipulation. In *ICRA*, pages 12462–12469. IEEE, 2024.
- [13] R. Geirhos, J.-H. Jacobsen, C. Michaelis, R. Zemel, W. Brendel, M. Bethge, and F. A. Wichmann. Shortcut learning in deep neural networks. *Nature Machine Intelligence*, 2(11):665–673, 2020.
- [14] A. Gunjal, J. Yin, and E. Bas. Detecting and preventing hallucinations in large vision language models. In *AAAI*, volume 38, pages 18135–18143, 2024.
- [15] J. Ho, A. Jain, and P. Abbeel. Denoising diffusion probabilistic models. *NeurIPS*, 33:6840–6851, 2020.
- [16] E. J. Hu, Y. Shen, P. Wallis, Z. Allen-Zhu, Y. Li, S. Wang, L. Wang, and W. Chen. LoRA: Low-rank adaptation of large language models. In *ICLR*, 2022.
- [17] P. Izmailov, P. Kirichenko, N. Gruver, and A. G. Wilson. On feature learning in the presence of spurious correlations. *NeurIPS*, 35:38516–38532, 2022.
- [18] S. Karamcheti, S. Nair, A. Balakrishna, et al. Prismatic vlms: Investigating the design space of visually-conditioned language model. In *ICML*, page 235, 2024.
- [19] S. Karamcheti, S. Nair, A. Balakrishna, et al. Prismatic vlms: Investigating the design space of visually-conditioned language models. In *ICML*, page 235, 2024.
- [20] M. J. Kim, K. Pertsch, S. Karamcheti, et al. Openvla: An open-source vision-language-action model. *arXiv preprint arXiv:2406.09246*, 2024.
- [21] A. Kirillov, X. Liu, and K. He. Segment anything model 2 (sam2). *arXiv preprint arXiv:2304.01492*, 2023.
- [22] S. Leng, H. Zhang, G. Chen, X. Li, S. Lu, C. Miao, and L. Bing. Mitigating object hallucinations in large vision-language models through visual contrastive decoding. In *Proceedings of the IEEE/CVF Conference on Computer Vision and Pattern Recognition*, pages 13872–13882, 2024.
- [23] Y. Leviathan, M. Kalman, and Y. Matias. Fast inference from transformers via speculative decoding. In *ICML*, pages 19274–19286. PMLR, 2023.
- [24] X. Li, K. Hsu, J. Gu, K. Pertsch, O. Mees, H. R. Walke, C. Fu, I. Lunawat, I. Sieh, S. Kirmani, et al. Evaluating real-world robot manipulation policies in simulation. *arXiv preprint arXiv:2405.05941*, 2024.
- [25] B. Liu, Y. Zhu, C. Gao, Y. Feng, Q. Liu, Y. Zhu, and P. Stone. Libero: Benchmarking knowledge transfer for lifelong robot learning. *NeurIPS*, 36:44776–44791, 2023.
- [26] F. Liu, K. Lin, L. Li, J. Wang, Y. Yacoob, and L. Wang. Mitigating hallucination in large multi-modal models via robust instruction tuning. *arXiv preprint arXiv:2306.14565*, 2023.
- [27] S. Liu, L. Wu, B. Li, et al. Rdt-1b: A diffusion foundation model for bimanual manipulation. *arXiv preprint arXiv:2410.07864*, 2024.

- [28] S. Liu, Z. Zeng, T. Ren, F. Li, H. Zhang, J. Yang, Q. Jiang, C. Li, J. Yang, H. Su, et al. Grounding dino: Marrying dino with grounded pre-training for open-set object detection. In *ECCV*, pages 38–55. Springer, 2024.
- [29] Z. Liu, C. Chi, E. Cousineau, N. Kuppaswamy, B. Burchfiel, and S. Song. Maniwav: Learning robot manipulation from in-the-wild audio-visual data. In *CoRL*, 2024.
- [30] Z. Liu, J. Wang, T. Dao, T. Zhou, B. Yuan, Z. Song, A. Shrivastava, C. Zhang, Y. Tian, C. Re, et al. Deja vu: Contextual sparsity for efficient llms at inference time. In *ICML*, pages 22137–22176. PMLR, 2023.
- [31] S. Lu, J. Chai, and X. Wang. Mitigating spurious correlations in zero-shot multimodal models. In *The Thirteenth International Conference on Learning Representations*, 2025.
- [32] T. O. M., D. Ghosh, H. Walke, et al. Octo: An open-source generalist robot policy. *arXiv preprint arXiv:2405.12213*, 2024.
- [33] A. Q. Nichol and P. Dhariwal. Improved denoising diffusion probabilistic models. In *ICML*, pages 8162–8171. PMLR, 2021.
- [34] M. Oquab, T. Darcet, T. Moutakanni, et al. Dinov2: Learning robust visual features without supervision. *Transactions on Machine Learning Research Journal*, 11:1–31, 2024.
- [35] Y. Park, D. Lee, J. Choe, and B. Chang. Convis: Contrastive decoding with hallucination visualization for mitigating hallucinations in multimodal large language models. In *AAAI*, volume 39, pages 6434–6442, 2025.
- [36] K. Pertsch, K. Stachowicz, B. Ichter, D. Driess, S. Nair, Q. Vuong, O. Mees, C. Finn, and S. Levine. Fast: Efficient action tokenization for vision-language-action models. *arXiv preprint arXiv:2501.09747*, 2025.
- [37] V. Rawte, A. Sheth, and A. Das. A survey of hallucination in large foundation models. *arXiv preprint arXiv:2309.05922*, 2023.
- [38] R. R. Selvaraju, M. Cogswell, A. Das, R. Vedantam, D. Parikh, and D. Batra. Grad-cam: Visual explanations from deep networks via gradient-based localization. In *ICCV*, pages 618–626, 2017.
- [39] R. Suvorov, E. Logacheva, A. Mashikhin, A. Remizova, A. Ashukha, A. Silvestrov, N. Kong, H. Goka, K. Park, and V. Lempitsky. Resolution-robust large mask inpainting with fourier convolutions. In *WACV*, pages 2149–2159, 2022.
- [40] O. M. Team, D. Ghosh, H. Walke, et al. Octo: An open-source generalist robot policy. *arXiv preprint arXiv:2405.12213*, 2024.
- [41] A. Telea. An image inpainting technique based on the fast marching method. *Journal of graphics tools*, 9(1):23–34, 2004.
- [42] H. Touvron, T. Lavril, G. Izacard, X. Martinet, et al. Llama: Open and efficient foundation language models. *arXiv preprint arXiv:2302.13971*, 2023.
- [43] H. Touvron, L. Martin, K. Stone, P. Albert, A. Almahairi, Y. Babaei, et al. Llama 2: Open foundation and fine-tuned chat models. *arXiv preprint arXiv:2307.09288*, 2023.
- [44] M. Varma, J.-B. Delbrouck, Z. Chen, A. Chaudhari, and C. Langlotz. Ravl: Discovering and mitigating spurious correlations in fine-tuned vision-language models. *NeurIPS*, 37:82235–82264, 2024.
- [45] D. Wan, J. Cho, E. Stengel-Eskin, and M. Bansal. Contrastive region guidance: Improving grounding in vision-language models without training. In *ECCV*, pages 198–215. Springer, 2024.
- [46] X. Wang, J. Pan, L. Ding, and C. Biemann. Mitigating hallucinations in large vision-language models with instruction contrastive decoding. *arXiv preprint arXiv:2403.18715*, 2024.
- [47] S. Wkeglarczyk. Kernel density estimation and its application. In *ITM web of conferences*, volume 23, page 00037. EDP Sciences, 2018.
- [48] B. Xie, J. Cao, J. Xie, F. S. Khan, and Y. Pang. Sed: A simple encoder-decoder for open-vocabulary semantic segmentation. In *CVPR*, pages 3426–3436, 2024.
- [49] W. Ye, G. Zheng, X. Cao, Y. Ma, and A. Zhang. Spurious correlations in machine learning: A survey. *arXiv preprint arXiv:2402.12715*, 2024.

- [50] M. Zawalski, W. Chen, K. Pertsch, O. Mees, C. Finn, and S. Levine. Robotic control via embodied chain-of-thought reasoning. *arXiv preprint arXiv:2407.08693*, 2024.
- [51] X. Zhai, B. Mustafa, A. Kolesnikov, and L. Beyer. Siglip: Sigmoid loss for language image pre-training. *arXiv preprint arXiv:2303.15343*, 2023.
- [52] X. Zhai, B. Mustafa, A. Kolesnikov, et al. Sigmoid loss for language image pre-training. In *ICCV*, pages 11975–11986, 2023.
- [53] Y. Zhang, C. Li, X. Wang, Y. Yang, A. Gupta, and T. Darrell. SpatialVLA: Exploring spatial representations for visual-language-action models. In *CVPR*, pages 14567–14578, 2024.
- [54] Q. Zhao, Y. Lu, M. J. Kim, Z. Fu, Z. Zhang, Y. Wu, Z. Li, Q. Ma, S. Han, C. Finn, et al. Cot-vla: Visual chain-of-thought reasoning for vision-language-action models. *CVPR*, 2025.
- [55] Z. Zhou, X. Ning, K. Hong, T. Fu, J. Xu, S. Li, Y. Lou, L. Wang, Z. Yuan, X. Li, et al. A survey on efficient inference for large language models. *arXiv preprint arXiv:2404.14294*, 2024.
- [56] J. Zhuang, J. Hu, L. Mu, R. Hu, X. Liang, J. Ye, and H. Hu. Falip: Visual prompt as foveal attention boosts clip zero-shot performance. In *ECCV*, pages 236–253. Springer, 2024.

A Appendix

A.1 CAM Visualization of Failure Cases.

We present the CAM [38] visualization of failure cases for the OpenVLA³ model across the nine tasks in Fig. 6. For each task, the averaged CAM results over the seven action dimensions (Δx , Δy , Δz , rot_x , rot_y , rot_z , gripper) are plotted. As can be observed from the figure, the model tends to predict actions based on spurious or background features in visual observations. For instance, on the “move the blue plastic bottle near sponge” (denoted as “Move Near”) task, the model habitually focuses on the “coke can” object that it frequently encountered during the training phase. These observations demonstrate that the learned policy utilizes perceptual data for decision-making in a way that significantly diverges from human strategies. Robot policies often erroneously associate task-irrelevant features with actions, a major cause of overfitting and poor generalization across tasks.

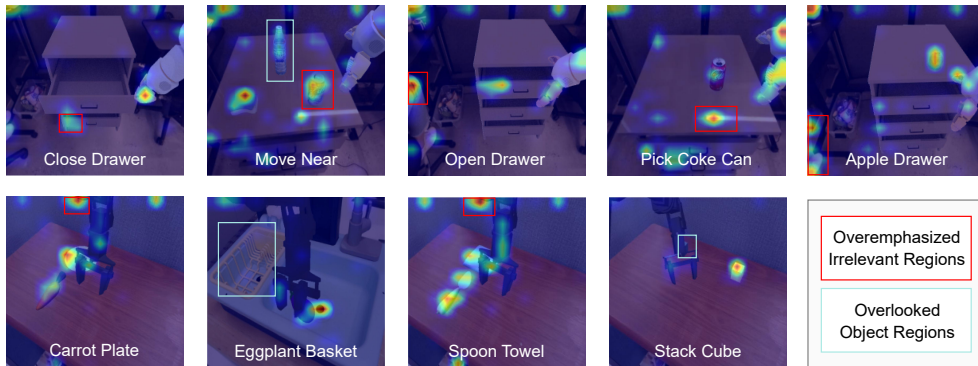


Figure 6: CAM visualization of failure cases.

A.2 Details of the Track2Mask Module

In our devised Track2Mask module, the target object specified by the language instruction in the initial observation can be annotated using Point and Box prompts, along with off-the-shelf open-vocabulary object detection models, as illustrated in Fig. 7. The SAM2 [21] model is then applied to automatically track and segment the target object across subsequent observations in the trajectory, which enables precise object masking with minimal or no human intervention during inference. Note that, once the task-specific objects are segmented by the SAM2 model, they are inpainted to create object-masked observations.

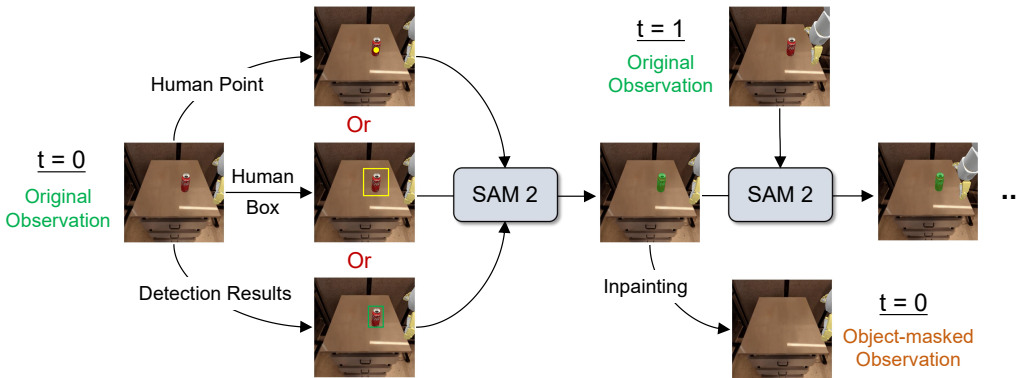


Figure 7: Illustration of the Track2Mask module.

³We only visualize the CAM results of OpenVLA, as the action prediction mechanism of diffusion-based models (e.g., Octo and π_0) makes it difficult to produce their CAM results.

A.3 Details of the Experimental Setup

A.3.1 Baseline Policies

Simulation Experiments. We conduct simulation experiments using three diverse robot policies in the SIMPLER environment, including the autoregressive policy OpenVLA [20], and diffusion-based policies Octo (base) [32] and π_0 [3].

- OpenVLA: a vision-language-action model with 7 billion parameters, is trained on 970,000 episodes of robotic demonstrations from the Open X-Embodiment dataset. This policy is fine-tuned using the pre-trained Prismatic [19] model.⁴
- Octo (base): an open-source generalist policy with 93 million parameters, is pre-trained on a blend of 25 different datasets from the Open X-Embodiment dataset. It utilizes a transformer backbone derived from ViT-B, accompanied by a diffusion action head to model expressive action distributions.⁵
- π_0 : a flow matching architecture built on top of a pre-trained vision-language model to leverage Internet-scale semantic knowledge. To facilitate evaluation in the SIMPLER environment, we leverage the reproduced version of π_0 , pretrained on tasks from this environment.⁶

Real-world Experiments. Since the simulation experiments show that π_0 significantly outperforms Octo and OpenVLA, we conduct real-world experiments using the π_0 policy ⁷. The policy is fine-tuned using on six real-world tasks, with each task consisting of 10 trajectories. We employ the parameter-efficient finetuning strategy LoRA [16] to adapt π_0 to these real world tasks. The training hyperparameters are listed in Table 2.

Table 2: Hyperparameters for finetuning π_0 on real-world tasks.

Hyperparameters	Setting
Batch Size	128
Optimizer	AdamW
Learning Rate	2.5e-5
LR Schedule	Cosine Decay
Weight Decay	1e-10
Training Step	25000
Action Chunk	10
LoRA Rank	16

A.3.2 Evaluation Tasks

We conduct extensive evaluations in both simulation and real-world environments using a total of 15 diverse tasks. The details of these tasks are presented in Table 3. We conduct 20 trials for each real-world task, randomizing the task configurations in every trial, as illustrated in Fig. 8.

A.4 Performance at the Maximum Step

In Table 1, tasks completed before the predefined maximum step are included in the success rate calculation, and the task is terminated upon completion. Table 4 presents success rates computed at the maximum step, irrespective of whether tasks were completed earlier. As seen, PCD demonstrates its advantages by improving the success rates of OpenVLA, Octo and π_0 by up to **33%**, **14%** and **7%**, respectively. We also observe that the vast majority of models underperform on these tasks relative to their results in Table 1, which indicates that even though they complete the task successfully ahead of the maximum steps, their later predicted actions lead to task failure. The superiority of the proposed PCD method is compellingly evidenced by the consistent performance gains over baseline policies presented in Table 1 and Table 4.

⁴<https://openvla.github.io/>

⁵<https://octo-models.github.io/>

⁶<https://github.com/allenzren/open-pi-zero>

⁷<https://www.physicalintelligence.company/blog/pi0>

Table 3: Details of simulation and real-world tasks.

Env.	Tasks	Language Instruction	Task-specific Objects	# Trials
Simulation	Close Drawer	close top/middle/bottom drawer	top/middle/bottom drawer	100
	Move Near	move X near Y	apple, orange, pepsi can, ...	100
	Open Drawer	open top/middle/bottom drawer	top/middle/bottom drawer	100
	Pick Coke Can	pick coke can	coke can	100
	Apple Drawer	open top drawer/place apple into top drawer	top drawer, apple	100
	Carrot Plate	put carrot on plate	carrot, plate	100
	Eggplant Basket	put eggplant into yellow basket	eggplant, yellow basket	100
	Spoon Towel	put the spoon on the towel	spoon, towel	100
Real-world	Stack Cube	stack the green cube on the yellow cube	green cube, yellow cube	100
	Pick Ball	pick the ball	ball	20
	Pick Plug	pick the plug	plug	20
	Move Near	move the can near the apple/watermelon	can, apple, watermelon	20
	Cookies Towel	put the cookies on the towel	cookies, towel	20
	Banana Plate	put the banana in the plate	banana, plate	20
	Stack Cube	stack the green cube on the yellow cube	green cube, yellow cube	20

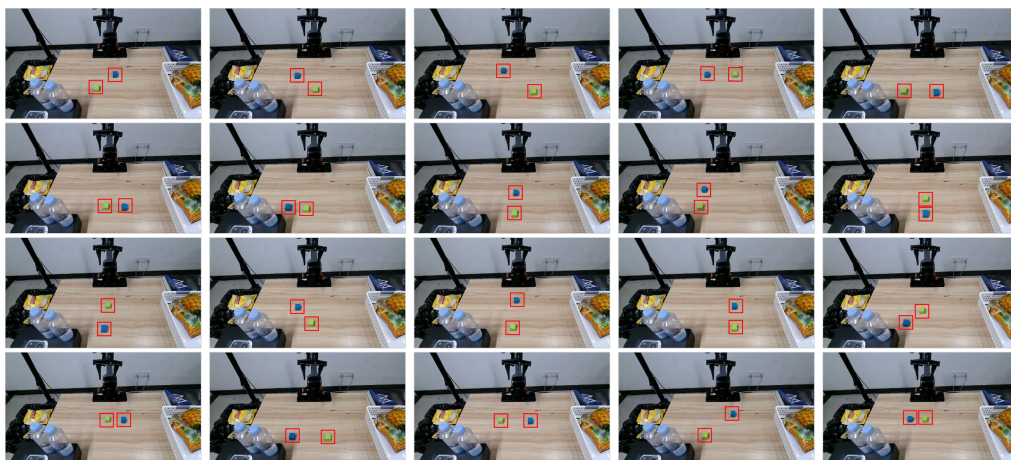


Figure 8: We conduct 20 trials for each real-world task, randomizing the task configurations in every trial. The language command for this task is “stack the green cube on the yellow cube.”

Table 4: Success rates (%) of three baseline policies integrated w/ or w/o our PCD over 9 tasks from Google Robot and WidowX—calculated at the maximum step.

Model	Base	OpenVLA[20]			Base	Octo [32]			Base	π_0 [3]			
		Point	Box	DINO		Point	Box	DINO		Point	Box	DINO	
Average	0.15	0.20	0.20	0.20	0.14	0.16	0.15	0.16	0.60	0.64	0.64	0.63	
		+33%	+33%	+33%		+14%	+7%	+14%		+7%	+7%	+5%	
Google Robot	Close Drawer	0.41	0.65	0.66	0.76	0.31	0.27	0.37	0.16	0.75	0.71	0.76	0.70
	Move Near	0.46	0.46	0.43	0.33	0.05	0.10	0.09	0.12	0.66	0.64	0.62	0.66
	Open Drawer	0.20	0.27	0.27	0.23	0.00	0.01	0.00	0.02	0.34	0.44	0.47	0.48
	Pick Coke Can	0.24	0.37	0.41	0.37	0.23	0.47	0.38	0.46	0.80	0.86	0.83	0.84
	Apple Drawer	0.00	0.00	0.00	0.00	0.00	0.00	0.00	0.00	0.11	0.29	0.24	0.22
WidowX.	Carrot Plate	0.00	0.02	0.00	0.03	0.10	0.18	0.16	0.12	0.56	0.62	0.57	0.56
	Eggplant Basket	0.01	0.01	0.02	0.08	0.47	0.32	0.28	0.40	0.91	0.80	0.80	0.83
	Spoon Towel	0.00	0.01	0.00	0.01	0.09	0.08	0.09	0.08	0.81	0.87	0.86	0.83
	Stack Cube	0.00	0.01	0.00	0.00	0.00	0.03	0.02	0.05	0.48	0.57	0.59	0.57